Modulating magnetic properties of a macrocyclic dinuclear copper(II) complex: Influence of counteranions on the crystal structure

Diego Venegas-Yazigi [a,*], Susana Cortés [a,b], Verónica Paredes-García [a,b,*], Octavio Peña [c], Andrés Ibañez [a], Ricardo Baggio [d], Evgenia Spodine [a]

[a] *CIMAT, Facultad de Ciencias Químicas y Farmacéuticas, Universidad de Chile, Of. 313, Olivos 1007, Independencia, Casilla 233, Santiago, RM, Chile*
[b] *Departamento de Química, Universidad Tecnológica Metropolitana, Av. José Pedro Alessandri 1242, Ñuñoa, Santiago, Chile*
[c] *UMR 6511 CNRS-Université de Rennes-1, 35042 Rennes Cedex, France*
[d] *Departamento de Física, Comisión Nacional de Energía Atómica, Av. Gral. Paz 1499, 1650 San Martín, Argentina*

Abstract

A group of dinuclear copper(II) compounds containing the macrocyclic complexes Cu_2L_{2+} ($LH_2 = C_{24}H_{28}N_4O_4$: a ligand derived from the condensation of 4-methyl-2,6-diformylphenol with 1,3-diamine-2-propanol) have been prepared, and characterised both structurally and magnetically. The compounds, containing different counterions, were formulated as: $[Cu_2LCl_2] \cdot 2H_2O$ (**1**); $[Cu_2L(\mu_2\text{-acetate})](acetate)$ (**2a**), $[Cu_2L(acetate)_2(H_2O)_2] \cdot 6H_2O$ (**2b**) and $[Cu_2L(H_2O)_2]_2(SO_4H) \cdot 2H_2O$ (**3**). The copper(II) ions present a square pyramidal geometry in three of the reported moieties, with axially coordinated halogens in **1**, *syn–syn* acetate ligands in **2b**, and water molecules in **3**. Compound **2a** is different in that the cations display distorted octahedral environments, with aqua and acetate oxygens at the apices. Compound **2b** which co-crystallised with **2a**, presents a folded structure of the macrocyclic ligand due to the presence of the bridging acetate molecule. There is a significant dependence of the bulk magnetic properties of the compounds studied with the nature of the counteranions used, evidenced in the large $-2J$ span observed throughout the series (306 to >1015 cm^{-1}). This might be due to the structural differences, both in molecular geometries as well as in crystal packing, introduced by the different counterions.

Keywords: Counteranions; Packing phenomena; Copper(II) macrocycles; Magnetism; Exchange phenomena; TIP

1. Introduction

The synthesis and solid state characterisation of novel macrocyclic phenoxo copper complexes are of interest due to their importance in the field of coordination chemistry, and because they represent the crossroads of two important research fields: molecular magnetism and macrocyclic chemistry [1–4]. In particular, magneto structural correlations in dinuclear copper(II) complexes bridged by hydroxide or alkoxide groups show that the major factor controlling the intramolecular spin coupling between the $S = 1/2$ metal centres is the Cu–O(R)–Cu angle. Ab initio calculations on simple model dimers examined the effect of the bridging angle, Cu–O distance, fold angle of the O–O axis, the solid angle at the oxygen bridge, and the degree of tetrahedral distortion at the copper centres, showing that the most relevant factor affecting exchange was the Cu–O–Cu bridging angle [5–8]. Experimental data have also been correlated with this latter geometrical parameter [9].

However, the design of new compounds to be used as new materials with pre-designed properties strongly depends on the solid state molecular structure and crystalline packing of the molecules [10–12]. Many physicochemical properties are mainly due to the molecular structure,

* Corresponding authors. Tel.: 56 2 9782801; fax: 56 2 9782868 (D. Venegas-Yazigi).
E-mail addresses: dvy@uchile.cl, fqi@ciq.uchile.cl (D. Venegas-Yazigi).

but other bulk properties like magnetic susceptibility may depend both on the molecular structure as well as on the solid state packing of the molecular entities.

In this work we present the structural and magnetic study of a group of dinuclear copper(II) macrocycles $[Cu_2L]^{2+}$, obtained with different counteranions, and where LH_2 is the ligand derived from the condensation of 2,6-diformyl-4-methylphenol and 1,3-diamino-2-propanol with different counteranions. The influence of the counteranion on the solid state molecular structure and the crystal lattice which define the bulk magnetic properties will be discussed. We present also an example of a butterfly distortion in on of the macrocycles, which takes place along the axis joining both copper centres, and which is assumed to produce a decrease in the value of the magnetic exchange coupling. There are examples in the literature of some μ-hydroxo dinuclear copper(II) complexes presenting a similar distortion, but along the line joining both hydroxo oxygens in which a decrease of the magnetic exchange coupling is also observed [13].

2. Experimental

2.1. Physical measurements

The diffuse reflectance UV–Vis spectra were recorded using a Perkin–Elmer Lambda 20 UV–Vis spectrophotometer equipped with a Labsphere RSA-PE-20 diffuse reflectance accessory. Magnesium oxide was used as reference and the spectra were recorded in the range of 1.0 and 6.0 eV at room temperature. Reflectance measurements were converted to absorption spectra using the Kubelka-Munk function F(R8).

Solution spectra were obtained with a UV–Vis spectrometer, Unicam UV3. Infrared spectra were recorded in KBr pellets using a Bruker Vector 22 FTIR instrument in the range 250–4000 cm^{-1}.

The magnetic susceptibility measurements were carried out on polycrystalline samples at CEPEDEQ, University of Chile with a Cryogenics Susceptometer-Magnetometer SQUID S-600, and at the Servei de Magnetoquímica of the Universitat de Barcelona and University of Rennes-1 with a Quantum Design SQUID MPMS XL.

2.2. Preparations

All reagents and solvents from commercial sources were used without further purification. The macrocyclic copper(II) complexes **1**–**3** were synthesised by the template method. A general synthetic procedure was used to obtain these complexes. In 20 mL of methanol, 2 mmol of 2,6-diformyl-4-methylphenol and 2 mmol of the corresponding copper(II) salts ($CuCl_2 \cdot 2H_2O$, $Cu(acetate)_2 \cdot H_2O$,

Table 1
Crystal and structure refinement data

Identification code	(**1**) $[Cu_2LCl_2] \cdot 2H_2O$	(**2**) $[Cu_2L(\mu_2\text{-ac})]$ (ac) $[Cu_2L(\mu\text{-ac})_2(H_2O)_2] \cdot 6H_2O$	(**3**) $[Cu_2L(H_2O)_2] \cdot 2SO_4H \cdot 2H_2O$
Empirical formula	$C_{24}H_{30}Cl_2Cu_2N_4O_6$	$C_{56}H_{80}Cu_4N_8O_{24}$	$C_{24}H_{36}Cu_2N_4O_{16}S_2$
Formula weight	668.50	1503.44	827.77
T (K)	296(2)	295(2)	297(2)
Wavelength (Å)	0.71073	0.71073	0.71073
Crystal system	triclinic	orthorhombic	triclinic
Space group	$P\bar{1}$ (#2)	*Pnma* (#62)	$P\bar{1}$ (#2)
a (Å)	7.7223(16)	15.1671(11)	7.727(5)
b (Å)	9.3901(19)	27.4366(19)	8.663(4)
c (Å)	10.167(2)	15.9786(11)	11.753(4)
α (°)	73.377(3)	90	82.199(6)
β (°)	85.768(4)	90	85.519(10)
γ (°)	65.766(3)	90	75.830(11)
V (Å^3)	643.4(2)	6649.2(8)	754.8(7)
Z	1	4	1
D_c (g cm^{-3})	1.725	1.502	1.817
μ (mm^{-1})	1.909	1.345	1.632
F(000)	342	3120	426
Crystal size (mm^3)	$0.30 \times 0.20 \times 0.02$	$0.42 \times 0.30 \times 0.20$	$0.50 \times 0.13 \times 0.08$
θ Range (°)	2.09–25.00	1.85–24.99	1.75–25.00
Index ranges	$-9 \leqslant h \leqslant 9$, $-11 \leqslant k \leqslant 11$, $-12 \leqslant l \leqslant 12$	$-17 \leqslant h \leqslant 18$, $-32 \leqslant k \leqslant 32$, $-18 \leqslant l \leqslant 18$	$-9 \leqslant h \leqslant 9$, $-10 \leqslant k \leqslant 10$, $0 \leqslant l \leqslant 13$
Data			
$N_{collected}$	4032	32776	4987
$N_{indep.}$, R_{int}	2246, 0.053	5974, 0.071	2616, 0.078
$N_{Obs.}$ [$I > 2\sigma(I)$]	1743	4549	2006
Number of independent reflections per parameters	12.1	12.1	11.3
Goodness-of-fit on F^2	1.099	1.116	0.944
R indices [$I > 2\sigma(I)$]	$R_1 = 0.0626$, $wR_2 = 0.1675$	$R_1 = 0.0629$, $wR_2 = 0.2017$	$R_1 = 0.0634$, $wR_2 = 0.1787$
R indices (all data)	$R_1 = 0.0794$, $wR_2 = 0.1753$	$R_1 = 0.0838$, $wR_2 = 0.2172$	$R_1 = 0.0792$, $wR_2 = 0.1883$
Largest peak and hole (e Å^{-3})	1.26, −0.69	0.95, −0.71	0.65, −0.77

$CuSO_4 \cdot 5H_2O$) were dissolved in methanol under nitrogen atmosphere. The green solution was refluxed for 2–3 h giving a green precipitate. Then 2 mmol of 1,3-diaminopropanol and 1 mL of triethylortoformiate were added to the reaction. The reaction mixture was refluxed for 8 h obtaining a green solution and a precipitate. The solid was filtered off and washed with small amounts of methanol. In the cases when no solid was obtained, a small amount of diethyl ether was added to induce the precipitation. All the complexes were dried under vacuum at 110 °C for 3 h. The microcrystalline solids were recrystallised from methanol.

$[Cu_2LCl_2] \cdot 2H_2O$ (**1**): yield: 24.3%. *Anal*. Calc. for $C_{24}H_{30}N_4O_6Cu_2Cl_2$: C, 43.12; H, 4.52; N, 8.38, Cu, 19.01. Found: C, 41.98; H, 4.41; N, 8.51, Cu, 18.92%. {$[Cu_2L(\mu_2\text{-acetate})]$(acetate) (**2a**) $[Cu_2L(acetate)_2(H_2O)_2]$

Table 2
Selected bond lengths (Å) and angles (°)

*(**1**)*			
Cu(1)–N(2)#1	1.957(5)	Cu(1)–O(1)#1	1.976(4)
Cu(1)–O(1)	1.959(4)	Cu(1)–Cl(1)	2.529(2)
Cu(1)–N(1)	1.965(6)		
N(2)#1–Cu(1)–O(1)	161.5(2)	N(1)–Cu(1)–O(1)#1	165.5(2)
N(2)#1–Cu(1)–N(1)	96.5(2)	N(2)#1–Cu(1)–Cl(1)	95.85(18)
O(1)–Cu(1)–N(1)	92.4(2)	O(1)–Cu(1)–Cl(1)	99.18(15)
N(2)#1–Cu(1)–O(1)#1	91.6(2)	N(1)–Cu(1)–Cl(1)	96.7(2)
O(1)–Cu(1)–O(1)#1	76.61(19)	O(1)#1–Cu(1)–Cl(1)	94.40(15)
*(**2a**)*			
Cu(1a)–O(1a)#3	1.967(4)	Cu(1a)–O(1a)	1.982(4)
Cu(1a)–N(1a)	1.974(4)	Cu(1a)–O(1W)	2.377(6)
Cu(1a)–N(2a)#3	1.975(4)	Cu(1a)–O(2a)	2.623(6)
O(1a)#3–Cu(1a)–N(1a)	169.28(17)	N(2a)#3–Cu(1a)–O(1W)	88.6(2)
O(1a)#3–Cu(1a)–N(2a)#3	93.19(16)	O(1a)–Cu(1a)–O(1W)	93.3(2)
N(1a)–Cu(1a)–N(2a)#3	96.93(19)	O(1a)#3–Cu(1a)–O(2a)	93.47(18)
O(1a)#3–Cu(1a)–O(1a)	77.15(16)	N(1a)–Cu(1a)–O(2a)	83.94(19)
N(1a)–Cu(1a)–O(1a)	92.63(17)	N(2a)#3–Cu(1a)–O(2a)	85.0(2)
N(2a)#3–Cu(1a)–O(1a)	170.24(17)	O(1a)–Cu(1a)–O(2a)	94.09(18)
O(1a)#3–Cu(1a)–O(1W)	93.5(2)	O(1W)–Cu(1a)–O(2a)	170.8(2)
N(1a)–Cu(1a)–O(1W)	90.3(2)		
*(**2b**)*			
Cu(1b)–N(1b)#2	1.961(4)	Cu(2b)–N(2b)	1.959(4)
Cu(1b)–N(1b)	1.961(4)	Cu(2b)–N(2b)#2	1.959(4)
Cu(1b)–O(1b)	1.963(3)	Cu(2b)–O(1b)#2	1.973(3)
Cu(1b)–O(1b)#2	1.963(3)	Cu(2b)–O(1b)	1.973(3)
Cu(1b)–O(2b)	2.225(5)	Cu(2b)–O(3b)	2.223(5)
N(1b)#2–Cu(1b)–N(1b)	96.7(2)	N(2b)–Cu(2b)–N(2b)#2	96.2(3)
N(1b)#2–Cu(1b)–O(1b)	165.02(17)	N(2b)–Cu(2b)–O(1b)#2	161.83(17)
N(1b)–Cu(1b)–O(1b)	91.77(15)	N(2b)#2–Cu(2b)–O(1b)#2	91.38(16)
N(1b)#2–Cu(1b)–O(1b)#2	91.77(15)	N(2b)–Cu(2b)–O(1b)	91.38(16)
N(1b)–Cu(1b)–O(1b)#2	165.02(17)	N(2b)#2–Cu(2b)–O(1b)	161.83(17)
O(1b)–Cu(1b)–O(1b)#2	77.5(2)	O(1b)#2–Cu(2b)–O(1b)	77.0(2)
N(1b)#2–Cu(1b)–O(2b)	101.66(15)	N(2b)–Cu(2b)–O(3b)	103.11(16)
N(1b)–Cu(1b)–O(2b)	101.66(15)	N(2b)#2–Cu(2b)–O(3b)	103.11(16)
O(1b)–Cu(1b)–O(2b)	88.62(15)	O(1b)#2–Cu(2b)–O(3b)	91.18(15)
O(1b)#2–Cu(1b)–O(2b)	88.62(15)	O(1b)–Cu(2b)–O(3b)	91.18(15)
*(**3**)*			
Cu(1)–N(2)#1	1.935(5)	Cu(1)–N(1)	1.960(5)
Cu(1)–O(1)#1	1.959(3)	Cu(1)–O(1W)	2.271(5)
Cu(1)–O(1)	1.961(4)		
N(2)#1–Cu(1)–O(1)#1	92.76(17)	O(1)–Cu(1)–N(1)	92.41(17)
N(2)#1–Cu(1)–O(1)	167.04(18)	N(2)#1–Cu(1)–O(1W)	92.3(2)
O(1)#1–Cu(1)–O(1)	75.93(16)	O(1)#1–Cu(1)–O(1W)	99.03(18)
N(2)#1–Cu(1)–N(1)	97.4 (2)	O(1)–Cu(1)–O(1W)	95.7(2)
O(1)#1–Cu(1)–N(1)	164.21(18)	N(1)–Cu(1)–O(1W)	92.6(2)

Symmetry transformations used to generate equivalent atoms throughout this work: (#1) $1-x, -y, 1-z$; (#2) $x, 1.5-y, z$; (#3) $1-x, 1-y, 1-z$; (#4) $1-x, -y, 2-z$; (#5) $x, 1+y, -1+z$; (#6) $-1+x, 1+y, -1+z$; (#7) $x, y, 1+z$; (#8) $-0.5+x, y, 0.5-z$; #9 $0.5+x, y, 0.5-z$; (#10) $0.5+x, y, 1.5-z$; (#11) $0.5-x, 1-y, 0.5+z$; (#12) $1-x, -y, -z$; (#13) $-1+x, -y, -z$; (#14) $1-x, -1-y, 1-z$; (#15) $2-x, -1-y, 1-z$; (#16) $-0.5+x, y, 1.5-z$.

(**2b**)}·$6H_2O$: yield: 45.3%. *Anal*. Calc. for $C_{56}H_{80}N_8O_{24}Cu_4$: C, 44.74; H, 5.36; N, 7.45, Cu, 16.91. Found: C, 45.83; H, 5.28; N, 7.63, Cu, 16.86%. $[Cu_2L(H_2O)_2]$-$2(SO_4H)\cdot 2H_2O$ (**3**): yield: 54%. *Anal*. Calc. for $C_{24}H_{36}N_4O_{16}Cu_2S_2$: C, 34.82; H, 4.38; N, 6.77, S, 7.75; Cu, 15.35. Found: C, 33.89; H, 4.28; N, 6.96, S, 7.96; Cu, 15.60%. The protonation of the sulfate anions is obviously due to the deprotonation of the phenolic groups during the complex formation reaction.

2.3. X-ray structure determination

Crystals of $[Cu_2LCl_2]\cdot 2H_2O$ (**1**); {$[Cu_2L(acetate)_2(H_2O)_2]$ $[Cu_2L(\mu_2\text{-acetate})]$}(acetate)·$6H_2O$ (**2a**,**2b**) and $[Cu_2L(H_2O)_2](SO_4H)_2\cdot 2H_2O$ (**3**) were glued with epoxy-resin on the tip of a capillary glass, and then mounted on a SMART-APEX Bruker diffraction system. Preliminary X-ray examination of the samples showed poor crystal quality, but cell determination was possible. A complete data set was measured for each compound [14], using 10 s by frame and 0.3° rotation between them. Reciprocal space exploration using RLATT [15] showed a main crystal plus secondary components for the complete series. The main component data was isolated and data reduction (SAINTPLUS [16]) and structure solution and refinement (SHELXTL [17]) was performed. Empirical absorption corrections were applied using SADABS [18]. Structures **2** and **3** present one of the amine-alcohol oxygen atoms disordered in two half-occupied positions (O13x and O13y in **2**, O12X and O12Y in **3**). Besides, in compound **2** there are a number of interstitial water molecules occupying depleted sites and whose occupations were refined and held constant in the last stages of refinement. Complex **3**, in turn presents a counterion with a severe rotational disorder. This was modelled using three partially occupied SO_4H moieties rotated around the sulphur centre and adding up to one complete sulphate unit.

In all cases hydrogen atoms attached to carbon were located at idealised positions. Some efforts were made in order to adequately find the position of those H atoms relevant for the H-bonding description. As a result, all those in structure **1** as well as a few (those pertaining to aqua molecules) in **2** and **3** could be trustfully inferred from a combined analysis of the Difference Fourier and the environment of potential acceptors for H-bonding. The resulting atoms were refined with metric restraints (O–H, 0.85(1) Å; H...H, 1.40(2) Å) and a riding isotropic displacement parameter. The remaining OHs could not be confidentially located and were accordingly disregarded from the model. Integrated information for all three

Table 3
H-bonding interactions and short contacts ascribable to H-bonding (O...O < 3.1 Å)

Compound	D	H	A	D–H (Å)	H...A (Å)	D...A (Å)	∠(DHA) (°)
1	O12	H12	Cl1#4	0.85(6)	2.20(6)	3.042(7)	170(8)
	O1W	H1Wa	Cl1#5	0.84(6)	2.34(6)	3.082(9)	146(8)
	O1W	H1Wb	O12#6	0.84(6)	2.51(6)	3.220(14)	142(11)
2	O1W	H1Wa	O2W	0.85(6)	2.35(6)	3.087(14)	144(6)
	O1W	H1Wb	O3a#3	0.85(6)	1.94(6)	2.643(10)	139(8)
	O2a		O12a			2.64	
	O12b		O2c#7			2.68	
	O13x		O3c#8			2.49	
	O2W		O12a#9			2.87	
	O2W		O6W			3.02	
	O2W		O7W			3.03	
	O3W		O3b#10			2.84	
	O3W		O12b			2.80	
	O4W		O3a			2.75	
	O4W		O5W#3			2.87	
	O4W		O6W#11			2.52	
	O4W		O7W#3			2.85	
	O5W		O2b#10			2.80	
	O5W		O13y			2.77	
	O7W		O13x			2.82	
	O7W		O2c			2.77	
	O8W		O12a#9			3.01	
3[a]	O1W	H1Wa	O2b	0.85(5)	2.06(5)	2.744(4)	137(4)
	O1W	H1Wb	O2W	0.85(4)	2.19(4)	2.865(8)	136(4)
	O12x		O2W#12			2.78	
	O12x		(SO_4)#12			(2.6–2.8)	
	O12y		O2W#13			3.00	
	O12y		(SO_4)#13			(2.7–2.8)	

See Table 2 for symmetry codes and Figs. 1–3 for atoms labelling.
[a] O...O contacts involving the disordered SO_4 groups reported as a range.

Table 4
π...π contacts

Compound	Group 1	Group 2	ipa (°)	ipd (Å)	ccd (Å)	sa (°)
1	C1 → C6	[C1 → C6]#14	0	3.47(1)	3.75(1)	22.3(1)
	C1 → C6	[C1 → C6]#15	0	3.43(1)	4.10(1)	33.2(1)
2	C1a → C6a	C1b → C6b	4.5(1)		3.68(1)	20(2)
	C1a → C6a	[C1b → C6b]#16	9.6(1)		4.37(1)	39(2)
3	C1 → C6	[C1 → C6]#15	0	3.55(1)	4.03(1)	28.3(1)
	C1 → C6	[C1 → C6]#14	0	3.39(1)	3.82(1)	27.5(1)

See Table 2 for symmetry codes and Figs. 1–3 for atoms labelling.
Column coding: ipa, interplanar angle; ipd, interplanar distance; ccd, centre-to-centre distance; sa, slippage angle [31].

structures (**1**–**3**), are presented in Table 1 (data collection, crystallographic and refinement details), Table 2 (selected bond length and angles), Table 3 (hydrogen bonds and short O...O contacts) and Table 4 (π...π interactions).

3. Results and discussion

3.1. Description of structures

3.1.1. $[Cu_2LCl_2]\cdot 2H_2O$ (**1**)

Fig. 1 presents a molecular drawing with the atom numbering for **1**, selected bond distances and angles are given in Table 2. The molecular structure corresponds to a binuclear copper(II) species with a Cu_2O_2 plane, which presents an inversion centre. Each copper atom shows a square pyramidal geometry, where the basal plane is formed by two nitrogen atoms from the macrocyclic ligand and two oxygen atoms, which are shared by both metallic atoms (Cu1–N1, 1.965(6) Å; Cu1–N2#1, 1.957(5) Å; Cu1–O1, 1.959(4) Å; Cu1–O1#1, 1.976(4) Å). The best mean plane through these atoms presents a maximum deviation of 0.040(1) Å for O1#1. The axial chloride ligand is 2.529(2) Å from this mean plane, and the copper(II) atom is shifted in the same direction in 0.22 (1) Å.

The macrocyclic ligand is made up of two parallel, almost planar halves, respectively, defined by O1, O12, N1, N2, C1–C9 and their corresponding centrosymmetric counterparts. These two groups are planar within a mean deviation of 0.03 and a maximum departure of 0.095(1) Å for O1 (O1#1), and displaced 0.66(1) Å from one another. The non-planar part is to be found in the C10–C12 group, with C1 1 presenting the most significant deviation, 0.29 (1) Å. The two centrosymmetric chloride atoms lay at 2.33(1) Å from their respective planes, while each copper(II) atom is shifted by 0.11(1) Å.

The fact that all those hydrogen atoms intervening in H-bonding could be located allowed a neat description of the H-bonding scheme. The main interactions are presented in Table 3: the one defined by the alcoholic hydrogen (H12) defines chains of (H-bonded) dimers running along the crystallographic *a*-axis, while those mediated by the hydration water ones H1Wa and H1Wb join these chains into 2D structures parallel to (0 1 0). Finally, the protruding phenyl groups in the L ligands fit into the open spaces left in neighbouring arrays, in such a way as to have the aromatic rings (forced by symmetry to be strictly parallel to each other) at a π–π interacting distances from one another. The details are presented in Table 4.

3.1.2. $\{[Cu_2L(acetate)_2(H_2O)_2]$ (**2a**) $[Cu_2L(\mu_2\text{-acetate})](acetate)$ (**2b**)$\}\cdot 6H_2O$

The crystalline structure of the acetate macrocyclic complex consists of two molecular forms, **2a** and **2b**. One of the complex molecules **2a** corresponds to a planar species with a Cu_2O_2 plane which presents an inversion centre (Fig. 2a), similar to the one observed for **1**. The geometry around each copper(II) centre can be described as highly distorted octahedral. The basal plane is similar to the one described for **1**, with copper–nitrogen and copper–oxygen distances being Cu1a–N2a#3, 1.975(4) Å; Cu1a–N1a, 1.974(4) Å Cu1a–O1a#3, 1.967(4) Å; Cu1a–O1a, 1.982(4) Å. The axial ligands are a water molecule (Cu1a–O1W, 2.377(6) Å) and a monodentate acetate ion (Cu1a–O2a, 2.623(6) Å), coordinated to each metal centre in a *trans* arrangement relative to the basal plane and subtending a O1W–Cu1a–O2a angle of 170.8(2)°. The fact that the acetate oxygen atom lays at a semi-coordinating distance from the metal centre allows an

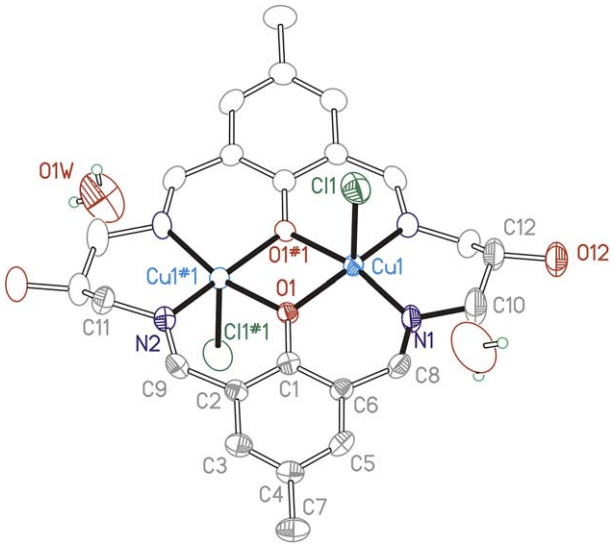

Fig. 1. Molecular diagram of **1**, with the independent and symmetry related parts, respectively, drawn as full and open displacement ellipsoids (40% probability level). In full solid bonds the copper coordination polyhedra. For symmetry codes, see Table 2 footnote.

alternative description of the environment around copper as being square-base pyramidal, with the aqua ligand occupying the apex.

As in the case of **1**, the macrocyclic ligand is composed of two planar sheets defined by O1a, N1a, N2a, C1a > C9a (and their centrosymmetric counterparts) parallel to each other at 0.30 Å from each other. Deviations from planarity of the individual halves are smaller than those found in **1** (with a maximum of 0.047 Å for O1a and a mean of 0.017 Å) as it is the shift between both planar moieties. The copper centres are "sandwiched" by these sheets, an lay at from 0.117(1) Å the nearest one.

The OH groups of the amine fragments of the planar macrocyclic complex **2** are axial and rest in a *trans* position with respect to the plane of the ligand. However, for complex **1** these same atoms are equatorial. A different ordering was reported from X-ray data by Tandon et al. [19], where a 4:1 equatorial to axial position of the hydroxo group of the diaminopropanol fragment of the macrocycle is mentioned.

The second binuclear copper(II) complex molecule **2b** (Fig. 2b) presents a folded macrocyclic ligand with a butterfly distortion [20]. Table 2 presents selected bond distances and angles. The acetate ligand bridges the copper(II) centres in a *syn–syn* mode, with two almost identical copper oxygen distances (Cu1b–O2b, 2.225(5) Å and Cu2b–O3b, 2.223(5) Å). This axial distance and the metal ligand atom distances are slightly shorter for the folded binuclear complex molecule, as compared to the planar one. A second acetate acts as counterion and balances

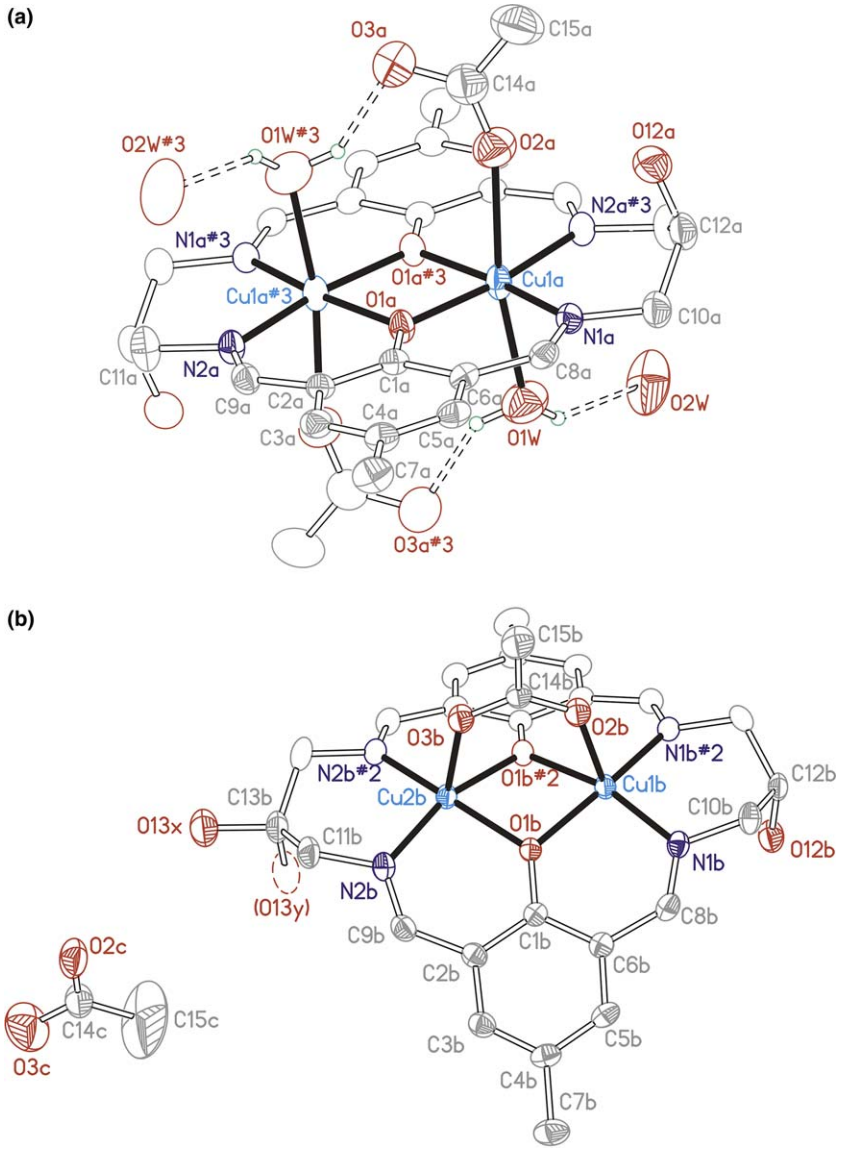

Fig. 2. Molecular diagram of **2**, with the independent and symmetry related parts, respectively, drawn as full and open displacement ellipsoids (40% probability level). In full solid bonds the copper coordination polyhedra. Disordered hydration water molecules not drawn, for clarity. For symmetry codes see Table 2 footnote. (a) Moiety **2a** $[Cu_2L(ac)_2(H_2O)_2]$: note the intramolecular H-bond connecting the aqua and the acetate groups. (b) Moiety **2b** $[Cu_2L(\mu_2\text{-ac})](ac)$: both positions for the split amine-alcohol oxygen shown, one of them in broken lines.

the charge of the complex species. The bond distances of copper oxygen and copper nitrogen atoms from the first coordination sphere are Cu1b–O1b, 1.963(3) Å and Cu1b–N1b, 1.961(4) Å.

The molecule possesses a crystallographic mirror plane containing the two copper atoms, the bridging acetate skeleton and the hydroxo groups of the diamine fragment of the macrocyclic ligand. This plane bisects the macrocycle, whose two planar halves (O1b, N1b, N2b, C1b > C9b, maximum deviation of 0.128(1) Å for O1b with a mean of 0.043(1) Å) are now far from parallel but define a dihedral angle of 46.9(1)°. Due to the intrinsic symmetry of the macrocycle, the molecule presents a non-crystallographic mirror plane, orthogonal to the former, which bisects the group along C7b, C4b, C1b, C14b, C15b, C7ba, C4ba, C1ba.

The crystal lattice presents six water molecules per molecule, disordered over several positions. The two unrelated dinuclear units organise as independent sets of columns, those containing Cu1a running along the *a*-axis, the remaining ones along *c*. These non-intersecting linear arrays define some kind of a 3D fabric, where the interleaving voids are filled by the free acetate anions as well as the disordered water molecules which act as connectors, via H bonding to the Os, OHs and water molecules in the columns. The existence of a large quantity of potentially good donors and acceptors for this type of interaction ensures a complex H-bonding scheme. Unfortunately, an accurate description of the H-bonding network was rendered impossible because of low data quality, which prevented finding many of the hydrogen atoms involved. An exception to this was the case of the aqua hydrogens, in particular H1Wb, the one making a strong intermolecular H-bond to the free O3c of the semi-coordinated acetate (Fig. 2b). The columns crossover is accomplished in such a way as to have the benzyl groups from the orthogonal, non-intersecting columns almost aligned along the *a* direction, with interplanar angles, centre to centre distances and slippage angles in the range 4–11°, 3.68(1)–4.37(1) Å and 20–40°, respectively. (For details see Table 4.) Thus the structure appears as stabilised by a large and varied quantity of non-bonding interactions.

3.1.3. $[Cu_2L(H_2O)_2](SO_4H)_2 \cdot 2H_2O$ (**3**)

Fig. 3 presents the molecular structure and atom numbering scheme for **3** and Table 2 presents selected bond distances and angles. For complex **3** the first coordination sphere of the copper atoms is square-base pyramidal, with the basal plane defined by the macrocycle (Cu1–N1, 1.960(5) Å; Cu1–N2#1, 1.935(5) Å; Cu1–O1, 1.961(4) Å; Cu1–O1#1, 1.959(3) Å) and the fifth position corresponding to the axial water ligand. This copper oxygen distance is 2.271(5) Å, being the shortest axial distance in the series of reported complexes. The least-square plane in the macrocyclic ligand is defined by N1–N2–O6–C1–C2–C3–C4–C5–C6–C7–C8–C9–C10 and the mean deviation of the atoms from this plane is 0.032 Å.

The crystalline structure presents isolated SO_4H counteranions, showing highly disordered oxygen atoms. These SO_4H groups form a chain along the *a*-axis. The existence of hydrogen bonds and van der Waals interactions, suggested by close contacts, stabilises the packing of the diaminopropanol fragment via hydrogen bonds.

Although the binuclear macrocyclic complex was prepared by the template reaction of 4-methyl-2,6-diformylphenol with 1,3-diamine-2-propanol in the presence of cupric sulphate, the counterions resulted to be two SO_4H species. The presence of two monovalent anions is evident by the experimental value of the percentage of the sulphur found for the complex, and X-ray diffraction data.

Again here the lack of precise information on some hydrogens, in addition to the severe disordered SO_4H counterions, turned the H-bonding description a rather speculative task, mainly based on the otherwise unexplainable short O...O contacts. Thus the counterion seems to serve as a double H-bonding bridge between neighbouring units, by accepting both an aqua (H1wa) and a diaminopropanol hydrogen. These interactions lead to the formation of H-bonded chains running along the *c*-axis, which present the benzyl group outwards, ready for a π–π interaction. This is achieved by the partial overlap of neighbouring chains when stacking along *a*. The resulting interaction is very similar to the ones already described (Table 4).

4. Spectral data

4.1. Infrared spectra

Selected IR data are presented in Table 5. All complexes show the same spectral pattern and the main differences

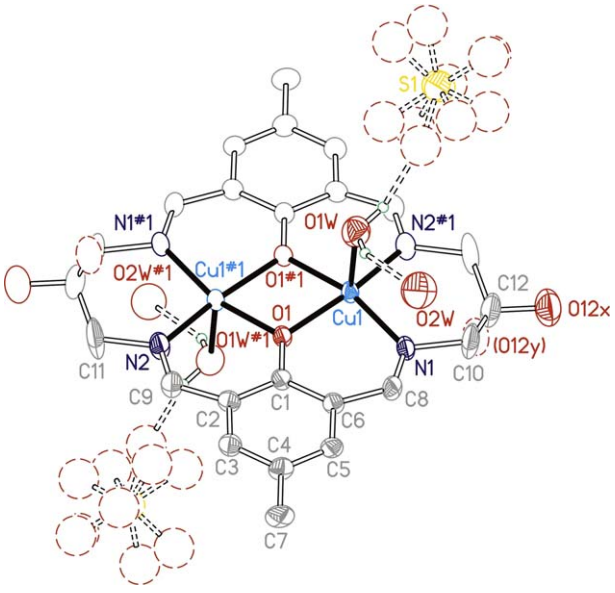

Fig. 3. Molecular diagram of **3**, with the independent and symmetry related parts, respectively, drawn as full and open displacement ellipsoids (40% probability level). In full solid bonds the copper coordination polyhedra. The disordered SO_4H counterions drawn as broken ellipsoids. Both depleted positions for the amine-alcohol oxygen shown, one of them in broken lines. For symmetry codes, see Table 2 footnote.

arise from absorptions due to the counteranions. Complex {**2a**,**2b**} shows stretching bands for the acetate ions at 1566 and 1408 cm^{-1}, corresponding to the asymmetric and symmetric absorptions of the carboxylate group, respectively. This allows to infer that the group is in its ionic form and also bridging the two metal atoms [21], in accordance to the structural data. Complex **3**, shows bands at 1113, 847 and 618 cm^{-1}; indicating the presence of the SO_4H species [21,22].

The complexes show the $\nu_{(C=N)}$ stretching bands in the range 1636–1639 cm^{-1} [23], and the $\nu_{C=C/C=N}$ ones between 1547 and 1568 cm^{-1}. The metal–ligand vibration zone shows three bands in all cases, one at 400 cm^{-1} assignable to the Cu–O stretching, and the remaining two at 350 and 370 cm^{-1} to the symmetric and asymmetric Cu–N vibrations [21].

4.2. Electronic spectra

All three reflectance spectra show a similar pattern, with strong electronic absorptions at 270, 390 and 420 nm attributed to the π–π^* ligand transitions [23]. The bands found at 352–363 nm are attributable to the phenolate-to-copper(II) charge-transfer band [2,5,24]. Much weaker, less defined absorption bands are found at lower energy (610–667 nm) associated to a d–d transitions [19].

Solution electronic spectra were recorded in methanol, and a similar pattern as for the reflectance spectra was obtained. All three copper(II) complexes show a very weak d–d transition band between 610–670 nm, indicative of a square pyramidal geometry [25–27]. Thus, it is possible to infer that the observed geometry of the binuclear copper(II) complexes in the solid state is maintained in solution.

5. Magnetic studies

Magnetic susceptibility measurements at variable temperature were performed for complexes **1**–**3**, in the temperature range 2–300 K. For compounds **1** and **3** measurements at different fields were also recorded. The results are summarised in Table 6, and presented as χ_M versus T plots in Figs. 4a and b (complexes **1** and **2**) and as χ'_M versus T plot in Fig. 4c (complex **3**). χ'_M corresponds to the molar magnetic susceptibility corrected by TIP.

The variable temperature–magnetic susceptibility data at 10 kOe for complex **1** were fitted with the Bleaney–Bowers equation, using the isotropic exchange Hamiltonian ($H = -2JS_1 \cdot S_2$) for the two interacting $S = 1/2$ centres [28]:

$$\chi_M(J,g,\rho,\theta) = \frac{2Ng^2\beta^2}{k(T-\theta)(3+e^{-2J/kT})}(1-\rho) + \frac{Ng^2\beta^2\rho}{4KT} + \mathrm{TIP} \quad (1)$$

where ρ is the fraction of paramagnetic impurity and θ corresponds to interdimer interactions.

The best fit to Eq. (1) gave $g = 2.175$, $2J = -1015$ cm^{-1}, $\rho = 0.025$, and $\theta = -5.0$ K ($10^3R = 5.9$). R is defined as $R = \left[\sum(\chi_{obs} - \chi_{calc})^2 / \sum \chi^2_{obs}\right]^{1/2}$. A TIP value of 6×10^{-4} emu mol^{-1} was used. Complex **1** presents a stronger antiferromagnetic behaviour as compared to the analogue $[Cu_2(UPM)Cl_2] \cdot 6H_2O$ ($2J = -722$ cm^{-1}), where $UPMH_2$ is the macrocyclic ligand formed by the condensation of 4-methyl-2,6-diformylphenol with 1,3-diaminepropane [29]. This ligand lacks the secondary alcohol group present in LH_2, and the reported complex presents slightly different

Table 5
Infrared vibrations for the copper(II) macrocyclic complexes (wavenumber in cm^{-1})

Complex	$\nu_{C=N}$	$\nu_{C=C/C=N}$	ν_{C-O} phenolic	ν_{C-H} aliphatic	δ_{C-H} iminic	δ chelate ring	ν_{Cu-N}	ν_{Cu-O}
1	1636 (s)	1568 (s)	1241 (m)	1436 (s)	821 (m)	500 (w)	376–356 (w)	465 (w)
2	1637 (s)	1566 (s)	1241 (m)	1437 (s)	822 (m)	500 (w)	378–351 (w)	478 (w)
3	1639 (s)	1547 (s)	[a]	1437 (s)	821 (m)	512 (w)	377–354 (w)	447 (w)

s, strong; m, medium; w, weak.
[a] The ν_{C-O} band is overlapped by the SO_4H ion absorptions.

Table 6
Comparative crystallographic and magnetic data for the binuclear copper(II) macrocyclic complexes

Compound	Axial ligand	Cu–Cu distance	Axial distance	Cu–O–Cu angle	Deviation of Cu[a]	$-2J$
$[Cu_2LCl_2] \cdot 2H_2O$	Cl	3.088	2.529	103.37	0.223	1015
$[Cu_2L(\mu\text{-}CH_3COO)]CH_3COO$	O^1	3.026	2.224 2.225	100.46		306
$[Cu_2L(CH_3COO)_2(H_2O)_2]$	O^2 O^3	3.087	2.624 2.376	102.86	0.109	921
$[Cu_2L(H_2O)_2] \cdot 2SO_4H \cdot 2H_2O$	O^3	3.091	2.271	104.08	0.042	
$[Cu_2L(H_2O)_2(NO_3)_2]$	O^4 O^3	3.097	2.586 2.429	102.05	0.033	631

Distance in Å, $2J$ in cm^{-1}.
[a] From ligand atoms plane N_2O_2 basal plane.

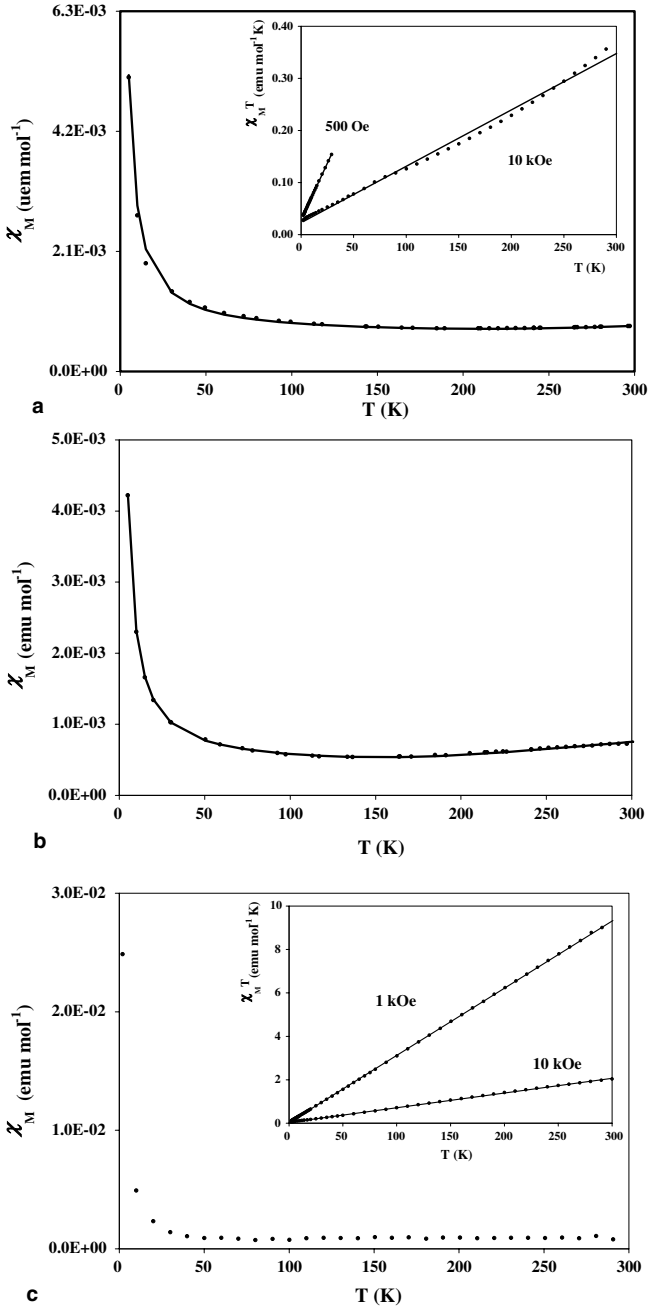

Fig. 4. Plots of χ_M vs. temperature for: (a) **1**; (b) **2a** and **2b**; (c) **3**. In (a) the solid line was calculated from Eq. (1), and in (b) the solid line was calculated from Eq. (2). In (c) $\chi'_M = (\chi_M - \text{TIP})$. Inset in (a) and (c) show a plot of $\chi_M \cdot T$ vs. T at different fields.

geometrical parameters: a copper–copper separation of 3.133 Å and a phenoxo bridge of 104.5°, as compared to 3.088 Å (Cu–Cu) and 103.34° (Cu–O–Cu) for **1**.

The magnetic data at 10 kOe for complex {**2a**,**2b**} was fitted with a modified Bleaney–Bowers equation, assuming that each binuclear macrocyclic copper(II) complex is characterised by a particular magnetic exchange constant, related to their different connectivities and distortions of the first coordination sphere. A TIP value of 3.8×10^{-4} emu mol^{-1} was considered for the fit of the data.

$$\chi^T_{MCu} = (\chi^1_M + \chi^2_M)(1-\rho) + \frac{N(g_1+g_2)^2\beta^2\rho}{4KT} + \text{TIP} \qquad (2)$$

For complex {**2a**,**2b**} the best fit to Eq. (2) gave $g_1 = 2.20$, $g_2 = 2.22$, $2J_1 = -306\ \text{cm}^{-1}$, $2J_2 = -921\ \text{cm}^{-1}$, $\rho = 0.021$, and $\theta = -15$ K ($10^2R = 1.2$).

Dihydroxo bridged dimers with butterfly distortions have been shown to present lower $2J$ parameters, than the completely planar systems [13]. In the reported dinuclear complexes the distortion occurs through the axis along both hydroxo oxygen atoms. This distortion produces a decrease in the overlap of the $d_{x^2-y^2}$ magnetic orbitals of the copper centres with the corresponding orbitals of the bridging phenoxo oxygen atoms, thus decreasing the antiferromagnetic interaction. This phenomenon has been explained theoretically by Kahn et al. [9]. In complex **2b** the distortion is induced by the μ-acetate coordination, along the axis through the copper centres. Therefore the intramolecular magnetic coupling in the non-planar $Cu_2O_{2(phenoxo)}$ system of complex **2b** should be described by the lower $2J$ value of $-306\ \text{cm}^{-1}$ and that of **2a** by the $2J$ value of $-921\ \text{cm}^{-1}$. The obtained parameters for **1** and **2a** are indicative of a strong antiferromagnetic coupling between the metal ions, which is commonly observed for this type of phenoxo bridged dicopper(II) complexes [5].

Complex **3** presents a high value for the measured susceptibility at 300 K. The inset of Fig. 4c shows the magnetic behaviour of this compound, which is assumed to correspond to temperature independent paramagnetism (TIP). The observed effect can not be attributed to paramagnetic impurities, since in such case the effect would have shown a behaviour independent of the applied field. However the observed phenomenon is shown to be dependent upon the magnitude of the applied field. The obtained TIP value from the $\chi_M T$ versus T plot is 308×10^{-4} emu mol^{-1} (1 kOe) and 68×10^{-4} emu mol^{-1} (10 kOe). From the corrected experimental susceptibility data, effective magnetic moments lower than the expected value for one unpaired electron (1.73 BM) per metal centre were obtained. It is important to remark that the Bleaney–Bowers equation was not used to fit the corrected susceptibility data for complex **3**, since this equation can fit the experimental data with different values for $2J$ and ρ parameters for extremely antiferromagnetic systems such as **3**.

Even though complex **3** and the reported $[Cu_2L(H_2O)_2](NO_3)_2$ [30] have similar pentacoordinated metal centres, with water molecules as axial ligands, the first is strongly antiferromagnetic with temperature independent paramagnetism, while the second has a pure intramolecular antiferromagnetic phenomenon with $2J = -631\ \text{cm}^{-1}$. The obtained magnetic data for **3**, together with aforementioned $2J$ value reported for the nitrate macrocyclic complex [30], clearly indicate that the lattice effects can play an important role on the magnitude of the magnetic exchange phenomenon.

A previous study of a family of compounds [29] with macrocyclic copper(II) complexes, derived from the

condensation of 4-methyl-2,6-diformylphenol with 1,3-diaminepropane and with different halogen axial ligands (Cl, Br, I) reports a trend of the intramolecular magnetic coupling with the nature of the coordinated halogen. Since the bulk geometry of the macrocycle is dependent on the nature of the halogen, it is not possible to infer that just the electronegativity of the axial ligand is responsible for the different magnetic behaviour. On the other hand, Tandon et al. [19] have also reported a rather high TIP value for a similar complex $[Cu_2L]$ with $Cu_2Cl_4^{2-}$ as counteranion.

We show in the present work that the nature of the counterion can play different roles, i.e., affecting the overall geometry of the macrocycle and acting, in some cases, as axial ligands. A dramatic example is observed in the acetate complex **2b** where the macrocycle is folded due to the presence of a bridging acetate anion. Therefore it is interesting to point out that the electronic and packing effects associated with the different anions can affect the bulk magnetic properties of the macrocyclic dinuclear copper(II) complexes.

6. Conclusions

While all the reported complexes can be described as pentacoordinated species with a square pyramidal geometry; the coordinated axial ligand depends on the nature of the counteranion of the used copper salt. The monodentate binding mode of the axial ligand generates planar macrocyclic complexes, while the *syn–syn* bridging mode of the acetate anion permits the formation of a folded macrocyclic moiety.

All the crystalline structures show the existence of a lattice with a great number of non-bonding interactions, such as hydrogen bonding and π–π stacking. All these interactions are due exclusively to the macrocyclic ligands, the solvate molecules and the different counteranions and not to the crystallisation conditions.

In the case of the planar species, the strongest antiferromagnetic exchange was observed for complex **3**, where the bisulphate anion is outside the first coordination sphere. The participation of the counteranion as axial ligand (compounds **1**, **2a**) produces a decrease in the antiferromagnetic exchange due to electronic interactions. Finally, dramatic distortions of the macrocycle are observed for compound **2b**, where the acetate anion is bridging the two metal centres and therefore the smallest $2J$ value is associated with this structure.

The reported binuclear complexes permit to asses that the existence of different bonding interactions of the anions, as those observed in the obtained crystalline structures, influence the bulk magnetic properties of the solid samples. Therefore counteranions should be considered relevant parameters for modulating magnetic properties.

Acknowledgements

Authors thank financial support from FONDAP (Grant 11980002) and ECOS-CONICYT (Grant C02E01). Fundación Andes is acknowledged for partially financing the purchase of the SMART-APEX Bruker diffraction system. We thank Prof. Jaime Llanos from Universidad Católica del Norte, Chile for recording the reflectance spectra. Authors thank Professors Joan Ribas and Dr. M. Salah El Fallah from Universitat de Barcelona, Spain, for important discussions and for magnetic measurements.

Appendix A. Supplementary data

Crystallographic data for **1**–**3** in the CIF format have been deposited with the Cambridge Crystallographic Data Centre, CCDC, 12 Union Road, Cambridge CB2 1EZ, UK. On request quote numbers 286700, 286701 and 286702. We provide comments for the structural refinement process. Packing of complexes **1**–**3** together with overlapping diagram of **2b** are available. Supplementary data associated with this article can be found, in the online version, at doi:10.1016/j.poly.2006.01.008.

References

[1] V. Fusi, A. Llobet, J. Mahia, M. Micheloni, P. Paoli, X. Ribas, P. Rossi, Eur. J. Inorg. Chem. 987 (2002).
[2] M. Thirumavalavan, P. Akilan, M. Kandaswamy, K. Chinnakali, G.S. Kumar, H.K. Fun, Inorg. Chem. 42 (2003) 3308.
[3] E. Ruiz, P. Alemany, S. Alvarez, J. Cano, Inorg. Chem. 36 (1997) 3683.
[4] E. Ruiz, S. Alvarez, P. Alemany, Chem. Commun. 2767 (1998).
[5] L.K. Thompson, S.K. Mandal, S.S. Tandon, J.N. Bridson, M.K. Park, Inorg. Chem 35 (1996) 3117.
[6] A.S. Borovik, Comm. Inorg. Chem. 23 (2002) 45.
[7] D. Braga, J. Chem. Soc., Dalton Trans. (2000) 3705.
[8] R. Robson, J. Chem. Soc., Dalton Trans. (2000) 3735.
[9] M.F. Charlot, O. Kahn, S. Jeannin, Y. Jeannin, Inorg. Chem. 19 (1980) 1410.
[10] H. Okawa, H. Furutachi, D.E. Fenton, Coord. Chem. Rev. 174 (1998) 51.
[11] E. Berti, A. Caneschi, C. Daiguebonne, P. Dapporto, M. Formica, V. Fusi, L. Giorgi, A. Gerri, M. Micheloni, P. Paoli, R. Pontellini, P. Rossi, Inorg. Chem. 42 (2003) 348.
[12] H. Grover, T.L. Kelly, L.K. Thompson, L. Zhao, Z. Xu, T.S.M. Abedin, D.O. Muller, A.E. Goeta, C. Wilson, J.A.K. Howard, Inorg. Chem. 43 (2004) 4278.
[13] S. Youngme, G.A. van Albada, O. Roubeau, Ch. Pakawatchai, N. Chaichit, J. Reedijk, Inorg. Chim. Acta 342 (2003) 48.
[14] SMART NT V5.625 Bruker AXS Inc., Madison, WI, USA.
[15] RLATT V3.0 Bruker AXS Inc. Madison, WI, USA.
[16] SAINTPLUS V6.22 Bruker AXS Inc., Madison, WI, USA.
[17] G.M. Sheldrick, SHELXTL NT/2000 Version 6.10., Bruker AXS Inc., Madison, WI, USA, 2000.
[18] SADABS V2.05 Bruker AXS Inc. Madison, WI, USA.
[19] S.S. Tandon, L.K. Thompson, J.N. Bridson, V. McKee, A. Downars, J. Inorg. Chem. 31 (1992) 4635.
[20] B. Dutta, P. Bag, U. Flörke, K. Nag, Inorg. Chem. 44 (2005) 147.
[21] K. Nakamoto, Infrared and Raman spectra of inorganic and Coordination Compounds, John Wiley & Sons, New York, USA, 1986.
[22] G. Socrates, Infrared Characteristic Groups frequencies, John Wiley & Sons, Great Britain, 1980.
[23] A. Aguiari, E. Bullita, U. Casellato, P. Guerriero, P.A. Vigato, Inorg. Chim. Acta 202 (1992) 157.

[24] B. Dutta, P. Bag, B. Adhikary, U. Flörke, K. Nag, J. Org. Chem. 69 (2004) 5419.
[25] R. Kannappan, R. Mahalakshmy, T.M. Rajendiran, R. Venkatesan, S. Rao, Proc. Indian Acad. Sci. (Chem. Sci.). 115 (2003) 1.
[26] S. Korupoju, N. Mangayarkarasi, S. Ameerunisha, E. Valente, P. Zacharias, J. Chem. Soc., Dalton Trans. (2000) 2845.
[27] C.R.K. Rao, P.S. Zacharias, Polyhedron 16 (1997) 1209.
[28] O. Kahn, Molecular Magnetism, Wiley-VCH Inc., USA, 1993.
[29] S.K. Mandal, L.K. Thompson, M.J. Newlands, E.J. Gabe, K. Nag, Inorg. Chem. 29 (1990) 1324.
[30] E. Spodine, Y. Moreno, M.T. Garland, O. Pena, R. Baggio, Inorg. Chim. Acta 309 (2000) 57.
[31] C. Janiak, J. Chem. Soc. Dalton Trans. (2000) 3885.